JACS
JOURNAL OF THE AMERICAN CHEMICAL SOCIETY

Article

pubs.acs.org/JACS

n-Type Water/Alcohol-Soluble Naphthalene Diimide-Based Conjugated Polymers for High-Performance Polymer Solar Cells

Zhihong Wu,[†] Chen Sun,[†] Sheng Dong,[†] Xiao-Fang Jiang, Siping Wu, Hongbin Wu, Hin-Lap Yip,* Fei Huang,* and Yong Cao

Institute of Polymer Optoelectronic Materials and Devices, State Key Laboratory of Luminescent Materials and Devices, South China University of Technology, Guangzhou 510640, PR China

Supporting Information

ABSTRACT: With the demonstration of small-area, single-junction polymer solar cells (PSCs) with power conversion efficiencies (PCEs) over the 10% performance milestone, the manufacturing of high-performance large-area PSC modules is becoming the most critical issue for commercial applications. However, materials and processes that are optimized for fabricating small-area devices may not be applicable for the production of high-performance large-area PSC modules. One of the challenges is to develop new conductive interfacial materials that can be easily processed with a wide range of thicknesses without significantly affecting the performance of the PSCs. Toward this goal, we report two novel naphthalene diimide-based, self-doped, n-type water/alcohol-soluble conjugated polymers (WSCPs) that can be processed with a broad thickness range of 5 to 100 nm as efficient electron transporting layers (ETLs) for high-performance PSCs. Space charge limited current and electron spin resonance spectroscopy studies confirm that the presence of amine or ammonium bromide groups on the side chains of the WSCP can n-dope $PC_{71}BM$ at the bulk heterojunction (BHJ)/ETL interface, which improves the electron extraction properties at the cathode. In addition, both amino functional groups can induce self-doping to the WSCPs, although by different doping mechanisms, which leads to highly conductive ETLs with reduced ohmic loss for electron transport and extraction. Ultimately, PSCs based on the self-doped WSCP ETLs exhibit significantly improved device performance, yielding PCEs as high as 9.7% and 10.11% for PTB7-Th/$PC_{71}BM$ and PffBT4T-2OD/$PC_{71}BM$ systems, respectively. More importantly, with PffBT4T-2OD/$PC_{71}BM$ BHJ as an active layer, a prominent PCE of over 8% was achieved even when a thick ETL of 100 nm was used. To the best of our knowledge, this is the highest efficiency demonstrated for PSCs with a thick interlayer and light-harvesting layer, which are important criteria for eventually making organic photovoltaic modules based on roll-to-roll coating processes.

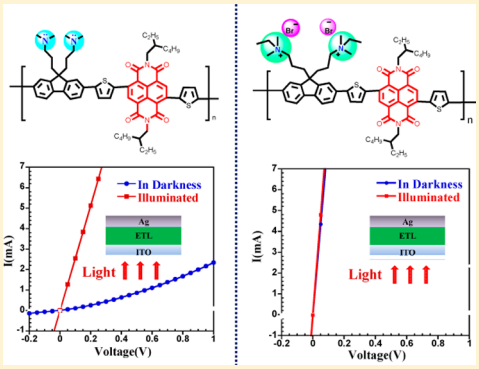

INTRODUCTION

Polymer solar cells (PSCs) based on the photoactive layer of a conjugated polymer donor and fullerene acceptor have attracted enormous attention in the past decades due to their various advantages in applications, including low-cost, lightweight, mechanical flexibility, and the potential of developing into large-area modules by solution processing.[1] Recently, much progress has been made in improving the performance of PSCs, with power conversion efficiencies (PCEs) of over 10% and 11% for small-area, single-junction and tandem PSCs, respectively.[2] To advance PSCs to a practical technology, however, several scientific and technological challenges must be overcome. It is well-known that large-area manufacturing in combination with high-throughput processing such as roll-to-roll (R2R) methods are the key advantages of PSCs, but the high PCEs demonstrated in the laboratory have not yet been successfully translated to large-area devices that can be fabricated via R2R processes. One of the main issues is the relative low charge mobility/conductivity of the organic semiconductors in PSCs compared to traditional inorganic semiconductors, which limit the use of relatively thin active layers (~100 nm) and interlayers (~5−50 nm) in most of the champion devices. However, to be compatible with R2R coating processes, it is critical to develop new materials with good charge mobility/conductivity that can work efficiently under thick film conditions, which can provide a better processing window to achieve high surface coverage and good film homogeneity.[3]

Water/alcohol-soluble conjugated polymers (WSCPs) have been successfully used as the interlayer materials in optoelectronic devices due to their many unique advantages.[4] They are usually processed from environmentally friendly solvents (such as alcohol), which is important for future industrial applications and can offer orthogonal solvent processability to prevent the solvent erosion problem during multilayer device fabrication. Moreover, the polar functional groups on the side chains of the polymers endow them with

Received: December 4, 2015
Published: January 22, 2016

DOI: 10.1021/jacs.5b12664
J. Am. Chem. Soc. 2016, 138, 2004−2013

excellent interfacial modification capability, which can enhance the charge collection from the active layer to the electrode.[5] Doping is typically required to improve the charge transport property of interlayers. A good example is the commonly used poly(3,4-ethylenedioxythiophene):poly(styrenesulfonate) (PEDOT:PSS) hole transport layer, in which the PEDOT is p-doped by a proton transfer mechanism and stabilized by the PSS polyanions and the doping concentration can be tuned to obtain films with varied conductivity.[6] Recently, a novel self-doping mechanism was introduced to develop p-type narrow-band gap conjugated polyelectrolyte WSCPs with cyclopenta-[2,1-b;3,4-b′]-dithiophene-*alt*-4,7-(2,1,3-benzothiadiazole) (CPDT-*alt*-BT) backbones and they were successfully applied as efficient hole transport layers in state-of-the-art single-junction and tandem PSCs.[7] Besides the development of new hole transport materials, more efforts have been dedicated to the development of WSCP-based ETLs to improve electron collection in PSCs.[8] One classic example is poly[(9,9-bis(3′-(*N*,*N*-dimethylamino)propyl)-2,7-fluorene)-*alt*-2,7-(9,9-dioctyl-fluorene)] (PFN),[9] which has been widely used as the cathode interlayers in optoelectronic devices, including all-printed polymer light-emitting displays,[10] state-of-the-art single-junction/tandem PSCs,[2h,11] and high-efficiency perovskite solar cells.[12] Despite their successful application as cathode interlayer materials, most of the WSCPs are based on polymers with an electron-rich conjugated backbone, which show relatively low electron mobility and therefore these WSCPs only work efficiently when a very thin film (<10 nm) is applied. Ideally, WSCPs based on an electron-deficient conjugated backbone with good electron transport properties are more suitable for use as efficient ETL for PSCs, but only a very few studies have reported on this type of WSCP.[13] Therefore, designing new n-type WSCPs and understanding their structure−property relationships are very important for the development of a new generation of cathode interfacial materials that is required to overcome the ultrathin interlayer bottleneck currently encountered in high performance PSCs. Recently, we have developed a new naphthalene diimide (NDI) based polymer as an efficient ETL to replace fullerenes in p-i-n planar-heterojunction perovskite solar cells, and it was found that a wide range of thicknesses of the new ETL can be applied to produce devices with high PCE owing to the good electron transport property of the polymer,[14] which triggered us to further design new polymer electron transporting materials as ETL for PSCs in this study.

Herein, we report the design and synthesis of two novel n-type WSCPs poly[(9,9-bis(3′-(*N*,*N*-dimethylamino)propyl)-2,7-fluorene)-*alt*-5,5′-bis(2,2′-thiophene)-2,6-naphthalene-1,4,5,8-tetracaboxylic-*N*,*N*′-di(2-ethylhexyl)imide] (PNDIT-F3N) and poly[(9,9-bis(3′-((*N*,*N*-dimethyl)-*N*-ethylammonium)propyl)-2,7-fluorene)-*alt*-5,5′-bis(2,2′-thiophene)-2,6-naphthalene-1,4,5,8-tetracaboxylic-*N*,*N*′-di(2-ethylhexyl)imide]dibromide (PNDIT-F3N-Br). Both PNDIT-F3N and PNDIT-F3N-Br contain a NDI-based conjugated main chain, with highly polar amino- or ammonium-functionalized side chains, respectively (Chart 1). The NDI based conjugated main chains endow the polymers with good electron mobility,[15] which have been used in transistors,[16] all polymer solar cells,[17] for diode transport,[18] battery,[19] and recently in perovskite solar cell.[14] The amino or ammonium functionalized side chains endow them with good processability from alcohol and also a unique interface modification capability to enhance electron collection in PSCs.[8e,20] Besides, SCLC and

Chart 1. Chemical Structures of PffBT4T-2OD, PTB7-Th, PNDIT-F3N, PNDIT-F3N-Br, PNDIT-F8 and $PC_{71}BM$

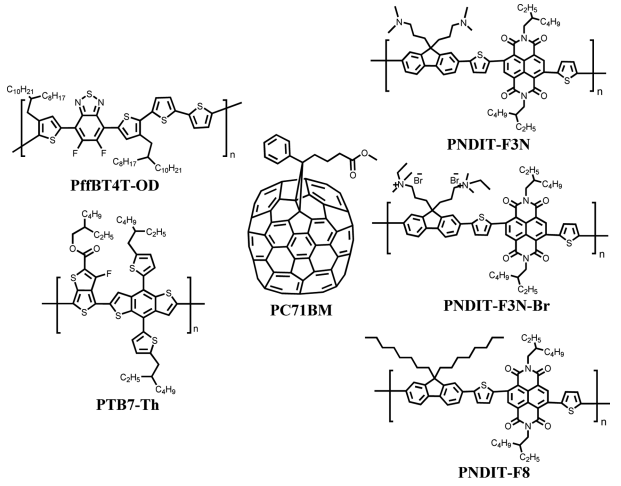

ESR studies indicate that both of these newly synthesized WSCPs possess a doping effect on $PC_{71}BM$. Furthermore, the ESR study results also reveal a self-doping effect among PNDIT-F3N and PNDIT-F3N-Br, which results in greatly improved electron transporting capability compared to that of their analogue copolymer poly[2,7-(9,9′-dioctylfluorene)-*alt*-5,5′-bis(2,2′-thiophene)-2,6-naphthalene-1,4,5,8-tetracaboxylic-*N*,*N*′-di(2-ethylhexyl)imide] (PNDIT-F8, Chart 1) without the amino or ammonium pendant group. More interestingly, photoconductivity studies indicate an obviously different doping mechanism between PNDIT-F3N and PNDIT-F3N-Br. PNDIT-F3N-Br exhibits the same high conductivity despite being in a dark or illuminated condition, whereas PNDIT-F3N displays distinct photo conductivity and exhibits further enhanced conductivity under light soaking. Both PNDIT-F3N and PNDIT-F3N-Br were used as the ETLs in PSCs with poly[[2,6′-4,8-di(5-ethylhexylthienyl)benzo[1,2-b;3,3-b]-dithiophene][3-fluoro-2[(2-ethylhexyl)carbonyl]thieno[3,4-*b*]-thiophenediyl]] (PTB7-Th) or poly[(5,6-difluoro-2,1,3-benzo-thiadiazol-4,7-diyl)-*alt*-(3,3‴-di(2OD)-2,2′;5′,2″;5″,2‴-quater-thiophen-5,5‴-diyl)] (PffBT4T-2OD) (Chart 1) as the donor material and $PC_{71}BM$ as the acceptor. Because of their excellent interface modification and electron transporting capabilities, the resulting devices exhibit promising performance with PCEs as high as 9.7% and 10.11% for PTB7-Th/$PC_{71}BM$ and PffBT4T-2OD/$PC_{71}BM$ systems, respectively. Moreover, investigation of the dependence of device performance on the ETL thickness shows both the open-circuit voltage (V_{oc}) and the fill factor (FF) of the resulting devices are largely maintained with a wider range of film thickness, and the PffBT4T-2OD/$PC_{71}BM$-based PSCs exhibit a prominent PCE of 8.04%, even when the ETL thickness is increased to 100 nm. Our results show that these NDI-based WSCPs are promising interlayer materials for PSCs and can potentially be used in R2R processed large-area optoelectronic devices that required a better processing window. More importantly, understanding the interesting and different doping behavior of these NDI-based WSCPs, caused by their different pendant side-chain groups, may provide more insights to further develop a new generation of self-doped n-type semiconductors for optoelectronic devices.

DOI: 10.1021/jacs.5b12664
J. Am. Chem. Soc. 2016, 138, 2004−2013

Scheme 1. Synthesis of n-Type WSCPs PNDIT-F3N, PNDIT-F3N-Br and n-Type Semiconducting Polymer PNDIT-F8

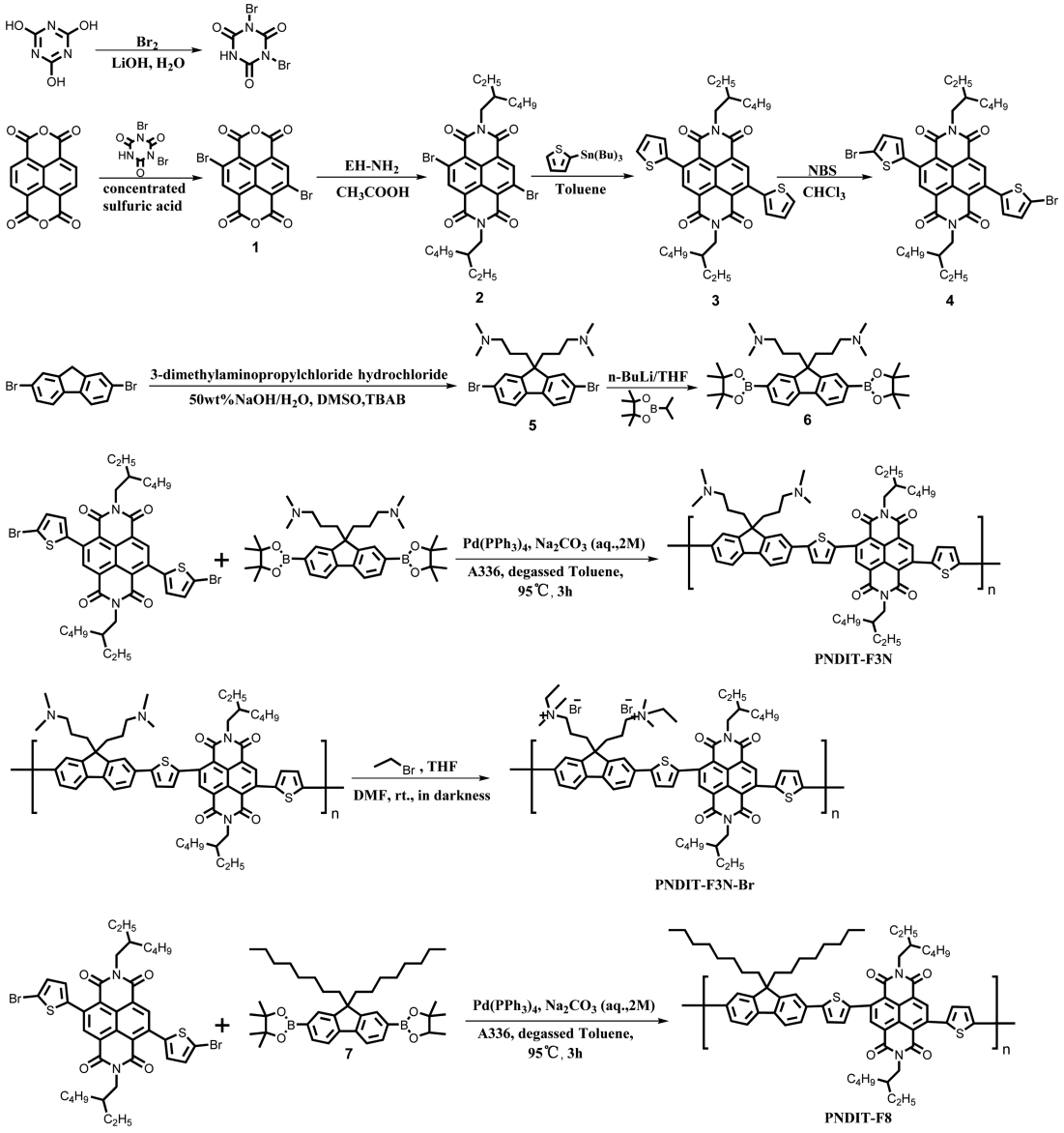

RESULTS AND DISCUSSION

Synthesis and Characterization. The synthesis of the new n-type copolymers is shown in Scheme 1. Monomers *N*,*N*′-bis(2-ethylhexyl)-2,6-bis(5-bromo-thiophen-2-yl)-1,4,5,8-naphthalenediimide[21] (4) 2,7-bis(4,4,5,5-tetramethyl-1,3,2-dioxaborolane-2-yl)-9,9-bis(6-(*N*,*N*-dimethylamino)-propyl)fluorine (6) and 2,7-bis(4,4,5,5-tetramethyl-1,3,2-dioxaborolan-2-yl)-9,9-dioctylfluorene (7) were synthesized and purified according to the published procedures.[22b] The new n-type NDI based amino-functionalized WSCP PNDIT-F3N was synthesized by the palladium-catalyzed Suzuki copolymerization of dibromo monomer (4) with monomer (6), whereas its ammonium-functionalized derivative PNDIT-F3N-Br was obtained by quaternizing the precursor polymer PNDIT-F3N with excess bromoethane in DMF solution at room temperature in darkness for 2 days. For comparison, their analogous polymer PNDIT-F8 with the same conjugated main chain but a different side chain was also made by the Suzuki copolymerization of monomers (4) and (7). The molecular structures of all monomers and copolymers were confirmed by ^{1}H nuclear magnetic resonance (NMR) spectroscopy. For the neutral polymer PNDIT-F3N in $CDCl_3$ solution, the signals corresponding to the methyleneamino and methylamino groups mixed together with the peaks for the methylene ($-CH_2-$) groups adjacent to the 9-position carbon atoms of the fluorene rings in the region around 2.15−2.02. After quaternizing with bromoethane, the signals for the methylene ($-CH_2N$, $-NCH_2CH_3$) and methyl ($-NCH_3$) groups adjacent to the nitrogen atoms shifted to the lower field region in DMSO-d_6 solution and could be distinguished from the methylene ($-CH_2-$) groups adjacent to the 9-position carbon atoms of the fluorene rings. Both PNDIT-F3N and PNDIT-F8 are readily soluble (solubility >30 mg/mL) in common organic solvents such as tetrahydrofuran (THF), chloroform, and toluene but insoluble in water and DMSO. The molecular weights of the copolymers were evaluated by gel permeation chromatography (GPC) measurement, which was carried out with THF as the eluent using linear polystyrene standards. The number-average molecular weight (Mn) of PNDIT-F3N and PDNIT-F8 was estimated to be 12.3 and 27 kg mol^{-1} with

DOI: 10.1021/jacs.5b12664
J. Am. Chem. Soc. 2016, 138, 2004−2013

Table 1. UV−Vis Absorption and Electrochemical Properties of the Polymers

polymers	λ_{abs}[a] [nm]	λ_{abs}[b] [nm]	E_{gap}[c] [eV]	E_{re} [V]	E_{ox} [V]	HOMO[d] [eV]	LUMO[e] [eV]
PNDIT-F3N	384 586	390 630	1.63	−0.41	1.22	−5.55	−3.91
PNDIT-F3N-Br	385 593	391 643	1.56	−0.31	1.14	−5.47	−4.18
PNDIT-F8	387 582	391 625	1.63	−0.43	1.30	−5.63	−3.89

[a]Solution. [b]Film. [c]Absorption onset. [d]$E_{HOMO} = -(E_{ox} + 4.33)$ eV. [e]$E_{LUMO} = -(E_{re} + 4.33)$ eV.

polydispersity index in the range of 1.7 and 1.3, respectively. The solubility of the quaternized polymer PNDIT-F3N-Br is different from its neutral precursor, polymer PNDIT-F3N-Br is insoluble in THF, chloroform, toluene and water, but exhibits limited solubility in ethanol (about 1 mg/mL), good solubility in DMSO (solubility >20 mg/mL), methanol (>15 mg/mL), and DMF (>20 mg/mL). It is worth noting that the amino-functionalized copolymer PNDIT-F3N is soluble in methanol and ethanol (both >12 mg/mL) in the presence of a small amount of acetic acid (about 0.1% in volume) due to a weak interaction between the nitrogen atoms in amino groups in the side chain and the acetic acid.[9,23] Consequently, both PNDIT-F3N and PNDIT-F3N-Br are good candidates as ETLs in PSCs, as they offer orthogonal solvent processability to prevent the solvent erosion problem during multilayer device fabrication. The thermal behavior of these copolymers was evaluated by differential scanning chromatography (DSC) and thermogravimetric analysis (see Figure S4−S5). The temperature was ramped from 40 to 800 °C at 10 °C/min in a nitrogen atmosphere. As depicted in Figure S4, the copolymer PNDIT-F8 shows a main decomposition with the onset temperature at 380 °C, while the two WSCPs exhibit at least two main degradation processes with the onset degradation temperature at 248 and 228 °C, respectively. The main decomposition of the copolymer PNDIT-F8 occurred when the side chains began to cleave, whereas for PNDIT-F3N, the first mass loss may due to the cleavage of the amino groups as the mass loss ratio is closed to the weight ratio of amino groups in the polymer. For polymer PNDIT-F3N-Br, the first mass loss is attributed to the decomposition of a quaternized ammonium group with release the ethyl bromide group.[22a] Thereafter both WSCPs underwent the second major degradation process owing to the cleavage of side chains, which is similar to previous reports.[22] As shown in Figure S5, DSC revealed no distinct exothermal transition for these copolymers in the second heating cycle over the temperature range of 30−180 °C, revealing that no crystalline behavior or phase transition occurred during this temperature section.

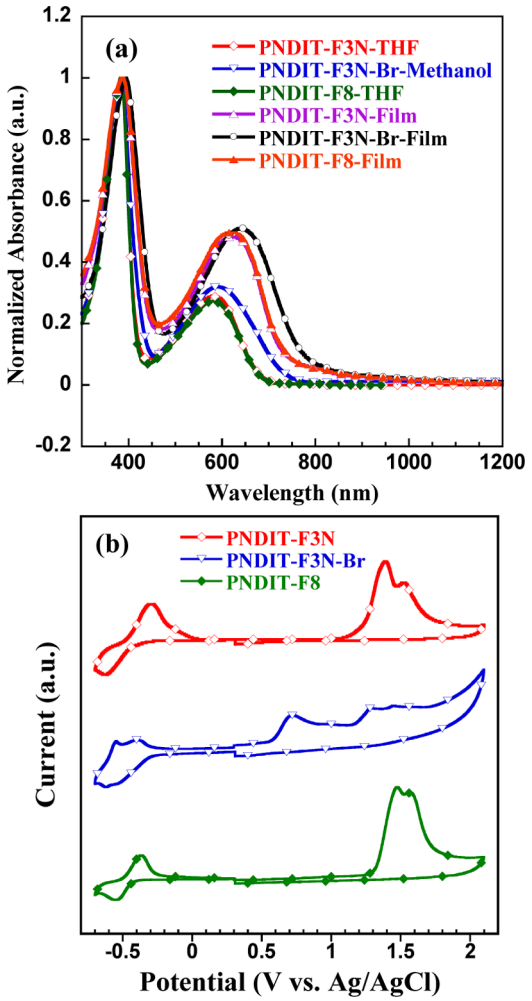

Figure 1. UV−vis spectra (a) and cyclic voltammograms (b) of the polymers.

Photophysical and Electrochemical Properties. The photophysical and electrochemical properties of the resulting copolymers are summarized in Table 1, and the corresponding UV−vis absorption spectra are shown in Figure 1a. All of the copolymers show two similar absorption bands, in which the first absorption peak below 500 nm is attributable to the characteristic absorbance of $\pi-\pi^*$ of the polymer backbones, and the low-energy absorbance in the region of 500−800 nm, is attributable to the intramolecular charge transfer (ICT) effects corresponding to the fluorene unit and electron-withdrawing NDIs. The amino-functionalized copolymer PNDIT-F3N exhibited almost the same absorption spectra, both in solution and in thin film, as its analogous copolymer PNDIT-F8, whereas the ICT absorption peak of the ammonium-functionalized copolymer PNDIT-F3N-Br was obviously red-shifted compared with PNDIT-F3N and PNDIT-F8. It is common for the conjugated polyelectrolytes to exhibit red-shifted absorption spectra in solution compared to their neutral precursor polymers, which may be due to the electrostatic perturbation by ions in close proximity to the optically active segment, solvatochromic effects arising from the polar solvent,[24] or multichain aggregation.[9] The thin-film absorption spectra were very similar to the solution spectra, but the longer wavelength (ICT) absorption bands were red-shifted and enhanced due to the increased conjugation and intermolecular interactions in the solid state. Moreover, a similar trend was observed with a red-shift in λ_{max} and λ_{onset} for the polyelectrolyte relative to its neutral precursor, and because no solvent was present, it is reasonable to speculate that the red-shifted absorption in the film was due to electrostatic modification of the ground-state electronic structure by the ion's Coulombic field, in spite of possible differences in coil structure and degree of aggregation cannot be ruled out.[25]

DOI: 10.1021/jacs.5b12664
J. Am. Chem. Soc. 2016, 138, 2004−2013

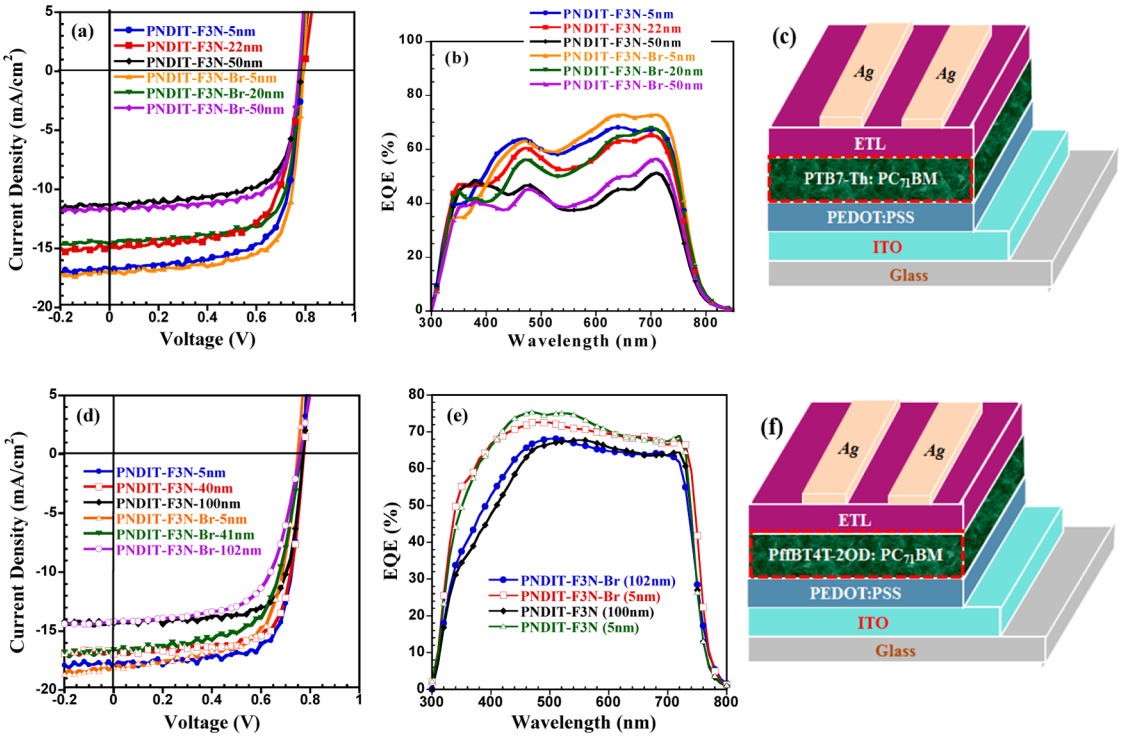

Figure 2. (a) $J-V$ curves of PSC devices using PTB7-Th:$PC_{71}BM$ as the active layer with different ETLs in various thickness. (b) EQE of the devices using PTB7-Th:$PC_{71}BM$ as the active layer with different ETLs in various thickness. (c) Device structure of the PTB7-Th:$PC_{71}BM$ BHJ based PSCs. (d) $J-V$ curves of PSC devices using PffBT4T-2OD:$PC_{71}BM$ as the active layer with different ETLs in various thickness. (e) EQE of the devices using PffBT4T-2OD:$PC_{71}BM$ as the active layer with different ETLs in various thickness. (f) Device structure of the PffBT4T-2OD:$PC_{71}BM$ BHJ based PSCs.

Cyclic voltammetry (CV) measurements were used to determine the frontier molecular orbitals of the copolymers in the thin films. The measurements were carried out under an inert atmosphere by using tetra-*n*-butylammoniumhexafluorophosphate (*n*-Bu_4NPF_6, 0.1 M in acetonitrile) as the supporting electrolyte with a glass carbon working electrode, a platinum wire counter electrode, and an Ag/AgCl electrode as the reference electrode. The ferrocene/ferrocenium (Fc/Fc^+) reference was used as an internal standard, which was assigned an absolute energy of −4.8 eV vs vacuum level.[26] Under the same experimental conditions, the onset potential of Fc/Fc^+ was measured to be 0.47 V with respect to the Ag/AgCl reference electrode. On the basis of the onset reduction potential with respect to the standard oxidation potential of the Fc/Fc^+, the lowest unoccupied molecular orbital energy levels (E_{LUMO}) and the highest occupied molecular orbital energy levels (E_{HOMO}) of the copolymers were calculated as $E_{LUMO} = -e(E_{re} + 4.33)$ (eV) and $E_{HOMO} = -e(E_{ox}+4.33)$ (eV) respectively,[27] where E_{re} (or E_{ox}) is the onset of the reduction (or oxidation) potential vs the Ag/AgCl reference electrode. The respective LUMO values of PNDIT-F8, PNDIT-F3N, and PNDIT-F3N-Br were estimated to be −3.89, −3.91, and −4.18 eV (Table 1). The relative lower LUMO value of PNDIT-F3N-Br may have been caused by electrostatic and anion-induced polarization due to the anion-π interaction between the bromine anion and the electron deficient aromatic units.[28] The low-lying LUMOs of polymers PNDIT-F3N and PNDIT-F3N-Br were very close to those of PCBM and $PC_{71}BM$, which can facilitate electron transportation from the fullerene acceptor to the cathode side. From the onset oxidation potential, the HOMO energy levels of PNDIT-F3N and PNDIT-F8 were determined to be −5.55 eV and −5.63 eV, respectively. It is worth noting that no signal for the oxidation of the pendant amino group was detected for PNDIT-F3N, which may be explained by the lone pair electrons on the nitrogen atom being prone to transfer onto the electron-deficient NDIs and leading to the formation of charge transfer complexes, a similar phenomenon was also observed in previous reports.[5,29] Polymer PNDIT-F3N-Br exhibited a clear oxidation process of the bromine anion with an onset oxidation potential of around 0.5 V before the oxidation of a conjugated main chain, which was verified by the oxidation of tetrabutylammonium bromide at the same applied potential in solution (see Figure S6), indicating that the bromine anions had much better electron-donating ability than the nitrogen atoms. Therefore, the HOMO level of the conjugated main chain of PNDIT-F3N-Br was calculated from the second onset oxidation potential and estimated to be −5.47 eV. These low-lying HOMO levels of the conjugated main chains indicate that the two WSCPs possess hole-blocking properties with respect to various donor materials in the photovoltaic devices.[30]

Performance of Bulk Heterojunction Polymer Solar Cells. To evaluate the performance of the new ETLs in PSCs, the devices were first investigated by fabricating and evaluating diodes with the configuration of indium tin oxide (ITO)/PEDOT:PSS/PTB7-Th:$PC_{71}BM$ (100 nm)/ETL/Ag (Figure 2c) with different cathode interfacial layers (PFN, PNDTI-F3N, and PNDIT-F3N-Br), which contain all-solution processed organic layers. Furthermore, to investigate the solvent effect on device performance,[31] reference devices with methanol treatment of the active layer were conducted, with all devices tested under a simulated AM 1.5G illumination at 100 mW/cm^2. As illustrated in Table S1, the performance of these devices increased from a PCE_{max} of 5.58% (short-circuit current

DOI: 10.1021/jacs.5b12664
J. Am. Chem. Soc. 2016, 138, 2004−2013

Table 2. Device Parameters of the PSCs Based on PTB7-Th/$PC_{71}BM$ with Different ETLs in Various Thicknesses under the Illumination of AM 1.5G, 100 mW cm^{-2}

ETL	V_{oc}(V)	J_{sc} (mA/cm^2)	FF (%)	PCE (%)	best PCE (%)
PNDIT-F3N					
5 nm	0.79 ± 0.01	16.32 ± 0.42	69.42 ± 1.35	8.8 ± 0.2	9.04
22 nm	0.79 ± 0.01	14.52 ± 0.40	66.56 ± 1.32	7.7 ± 0.1	7.79
50 nm	0.78 ± 0.01	10.98 ± 0.41	68.24 ± 1.62	5.8 ± 0.2	6.03
PNDIT-F3N-Br					
5 nm	0.79 ± 0.01	16.62 ± 0.37	71.14 ± 1.10	9.5 ± 0.2	9.70
20 nm	0.78 ± 0.01	14.33 ± 0.38	70.62 ± 1.25	7.7 ± 0.4	8.08
50 nm	0.78 ± 0.01	11.41 ± 0.40	70.18 ± 1.27	6.3 ± 0.2	6.45

Table 3. Device Parameters of the PSCs Based on PffBT4T-2OD/$PC_{71}BM$ with Different ETLs in Various Thicknesses under the Illumination of AM 1.5G, 100 mW cm^{-2}

ETL	V_{oc}(V)	J_{sc} (mA/cm^2)	FF (%)	PCE (%)	best PCE (%)
PNDIT-F3N					
5 nm	0.75 ± 0.00	18.38 ± 0.49	65.91 ± 1.15	9.1 ± 0.3	9.42
40 nm	0.76 ± 0.01	16.58 ± 0.39	64.31 ± 2.54	8.1 ± 0.2	8.33
100 nm	0.76 ± 0.00	16.12 ± 0.55	62.31 ± 0.84	7.6 ± 0.2	7.97
PNDIT-F3N-Br					
5 nm	0.77 ± 0.00	17.64 ± 0.27	72.29 ± 1.20	9.8 ± 0.2	10.11
41 nm	0.77 ± 0.00	16.48 ± 0.35	72.85 ± 0.41	9.3 ± 0.2	9.61
102 nm	0.77 ± 0.00	14.28 ± 0.30	71.48 ± 1.24	7.9 ± 0.2	8.04

density (J_{sc}) = 16.42 mA/cm^2, open-circuit voltage (V_{oc}) = 0.67 V, fill factor (FF) = 54.42%) for methanol, to 8.98% (J_{sc} = 16.58 mA/cm^2, V_{oc} = 0.80 V, FF = 69.32%) for PFN, to 9.04% (J_{sc} = 16.74 mA/cm^2, V_{oc} = 0.80 V, FF = 70.77%) for PNDIT-F3N, and eventually to 9.7% (J_{sc} = 16.99 mA/cm^2, V_{oc} = 0.80 V, FF = 72.24%) for PNDIT-F3N-Br, demonstrating that the NDI-based WSCPs are a promising type of ETL. Moreover, the dependence of device performance on ETL thickness was investigated by spin-coating polymer solutions of varying concentrations onto an active layer to produce ETLs over a thickness range of 5 nm to nearly 100 nm. The current density−voltage (J−V) characteristics of devices are provided in Figure 2a, and the photovoltaic characteristics are summarized in Table 2. As Figure 2a shows, although the performance of the device declines gradually with increasing ETL thickness, no S-shaped J−V kink is present, indicating no evident enhancement of the series resistance R_s of the devices.[29d] This is further evidenced by the dark-current J−V curves as the curves remain unchanged despite the change in the thickness of the ETLs (see Figure S7−S8). From Table 2, it can be clearly determined that the degradation of the PCEs is mainly due to the decline of J_{sc}, whereas V_{oc} and FF are basically unchanged.

We further investigated the external quantum efficiency (EQE) of devices with various ETL thicknesses. In Figure 2b, a major decline in the EQE can be observed in the 500−800 nm section, which is exactly covered by the ICT absorption band of PNDIT-F3N. Thereby, we supposed that the suppressed reflectance in the 500−800 nm range for devices with thicker ETLs might be responsible for the reduced J_{sc}. Nevertheless, the thick BHJ composite layers play a more significant role in R2R manufacturing processing, and thus the potential of these ETLs was further evaluated for broader device application. We then more intensively investigated another BHJ system (PffBT4T-2OD/$PC_{71}BM$), which could be processed in a wide thickness to minimize the absorption loss in the active layer. As shown in Table 3, there was less than 20% loss of PCE for devices fabricated with ETL thicknesses ranging from 5 to 100 nm for PNDIT-F3N-Br, and for PNDIT-F3N, the corresponding loss of PCE was around 15%. In the PTB7-Th/$PC_{71}BM$ system, the loss is around 50%, and moreover, the EQE spectrum data of the PffBT4T-2OD/$PC_{71}BM$-based devices further demonstrate that with the thicker film of the active layer the effect of the thickness of the ETL on J_{sc} will be reduced due to the light being absorbed in the active layer (see Figure 2e). These results indicate that the newly synthesized n-type WSCPs are a promising type of ETL for the R2R processing of PSCs. Consequently, a prominent PCE of 8.04% (J_{sc} = 14.58 mA/cm^2, V_{oc} = 0.77 V, FF = 72.72%) with an ETL thickness of 100 nm was achieved and an outstanding PCE of 10.11% (J_{sc} = 17.91 mA/cm^2, V_{oc} = 0.77 V, FF = 73.49%) with optimized ETL thickness was realized. To the best of our knowledge, this is the first report of WSCP ETLs that can be processed in 100 nm thickness and in which the PCE still surpasses 8%.

The surface topographic features of the various ETLs were examined by atomic force microscopy (AFM). All samples were spin-coated from the polymer solutions in methanol onto active layers under the same condition as used in device fabrication. The AFM spectra are provided in the Supporting Information (see Figures S11−S12). As the thickness increased, the root-mean-square values of both of the WSCP films exhibited the same decreasing trend within a small range of amplitudes, indicating the thick-film ETLs can smooth the surface of active layers, which is advantageous for improving device performance. In addition, compared to the PffBT4T-2OD/$PC_{71}BM$ BHJ system, films on the PTB7-Th/$PC_{71}BM$ BHJ layer were observed to be slightly rougher but showed no significant difference, implying that the surface morphologies of these devices have a negligible influence on device performance.

Scanning Kelvin Probe Microscopy Study. The effect of the thickness of the WSCPs on the work function (WF) of the Ag electrode was studied by scanning Kelvin probe microscopy, and the results are summarized in Table 4. The WF of the bare Ag was measured to be 4.66 eV, and after deposition of an

DOI: 10.1021/jacs.5b12664
J. Am. Chem. Soc. 2016, 138, 2004−2013

Table 4. Scanning Kelvin Probe Microscopy (SKPM) of Different ETLs Treated Ag Electrodes

electrode	thickness of ETLs/work function		
Ag	4.66 eV		
Ag/PFN	5 nm/4.19 eV		
Ag/PNDIT-F3N	5 nm/4.20 eV	50 nm/4.04 eV	100 nm/3.95 eV
Ag/PNDIT-F3N-Br	5 nm/3.93 eV	50 nm/3.93 eV	100 nm/3.94 eV

ultrathin layer (5 nm) of different ETLs, including PFN, PNDIT-F3N, and PNDIT-F3N-Br, the WF decreased to 4.19, 4.20, and 3.93 eV, respectively. The variation in WFs among the WSCP-treated electrodes resulted from the different polar nature of the terminal groups on the WSCP. This suggests that the quaternary ammonium derivatives could form larger interfacial dipoles at the electrode when compared to the amine group, leading to better ohmic contact at the cathode. To further investigate the effect of thickness of the ETLs on the WF tuning ability of the Ag electrodes, various thicknesses of the ETLs from 5 to 100 nm were applied, and the corresponding WFs of the modified electrodes are summarized in Table 4. We observed that the WFs of the PNDIT-F3N-Br-modified electrodes were independent of the thickness of the ETL, whereas the WFs of the PNDIT-F3N-modified electrodes reduced subsequently from 4.20 to 3.95 eV with increasing film thickness. A similar effect was also reported in the cases of other amine-functionalized conjugated polymers.[32] The performance of the PSCs showed dependency on the WF of the Ag cathode, and at low thickness (5 nm), PSCs based on the PNDIT-F3N-Br ETL showed obviously higher PCEs than the PNDIT-F3N-based devices (Tables 2 and 3). However, when the ETL thickness increased to 50−100 nm, at which point the WF of the Ag cathode is similar for both cases, the PSCs based on the two different ETLs showed comparable performance. The flexibility of using a relatively thick ETL and also a more stable and possibly printable Ag as the cathode paves the way for eventually using all-printing processes to fabricate the PSCs.

Space Charge Limited Current and Electron Spin Resonance Spectroscopy Study. To study the charge transport properties of the ETLs, electron-only devices based on the architectures of ITO/Al/ETL/Al were prepared and the electron mobilities of the ETLs were extracted by fitting the data using the SCLC model.[33] The electron mobility of sole $PC_{71}BM$, PNDIT-F3N, and PNDIT-F3N-Br calculated from the SCLC curves shown in Figure 3b are at the same orders of magnitude and were determined to be 7.1×10^{-4}, 2.5×10^{-4}, and 2.6×10^{-4} cm^2 V^{-1} s^{-1}, respectively. Because a few reports have suggested that amines and ammonium salts may possibly n-dope fullerenes with enhanced conductivity,[29a] we further evaluated the contact properties between the $PC_{71}BM$ and the ETLs by testing the electron-only devices with the structure of ITO/Al/$PC_{71}BM$/ETL/Al, as shown in Figure 3a. In comparison with the sole layer of $PC_{71}BM$, the current densities of the $PC_{71}BM$/ETL (5 nm) bilayer films at low voltages were two to 3 orders of magnitude higher (Figure 3c), indicating that the electrical conductivities of the films were improved by possible n-doping of the $PC_{71}BM$ at the $PC_{71}BM$/ETL interface. In addition, the SCLC electron mobilities of the devices were determined to be 1.2×10^{-3} and 2.0×10^{-3} cm^2 V^{-1} s^{-1} for the $PC_{71}BM$/PNDIT-F3N and $PC_{71}BM$/PNDIT-F3N-Br films, respectively, which are much higher than those of the pure films. The improved mobilities may be due to the removal of the $PC_{71}BM$ surface traps through n-doping, which

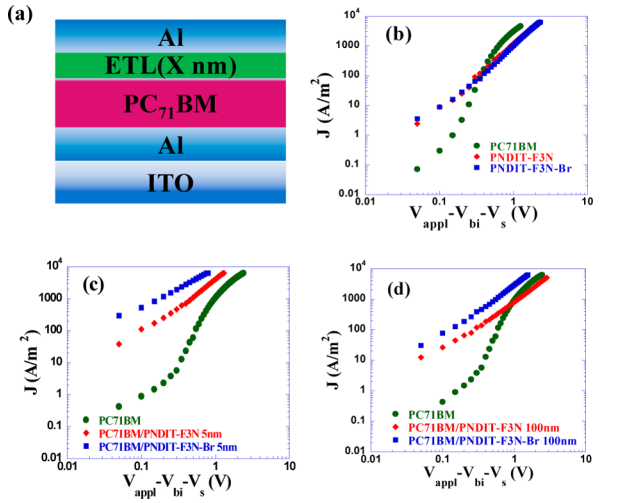

Figure 3. Structure of electron only devices (a) and $J-V$ curves of electron only devices (b−d).

reduces the transient time of the electrons through the film.[20c] It is noteworthy that this improvement in the electrical properties was also observed when the thickness of the ETLs was increased to 100 nm (Figure 3d). The current density of the devices remained ten times higher than that of the sole $PC_{71}BM$ device under the equivalent voltage V ($V = V_{appl} - V_{bi} - V_s$). These results suggest that achieving electrically coherent contact between the $PC_{71}BM$ and ETL through the interfacial n-doping is an important factor that contributes to the overall improvement of the performance of the PSCs.[5,29b,c]

To provide further evidence on the electron transfer from the amino groups or bromide anions to $PC_{71}BM$, an ESR spectroscopy study was performed. A reference polymer PNDIT-F8 with pure alkyl side chains was also tested as it is composed of the same backbone structure as PNDIT-F3N and PNDIT-F3N-Br, and all samples were studied in solid form and in darkness. We first investigated the sole component of PNDIT-F8, PNDIT-F3N, and PNDIT-F3N-Br. No ESR signal was detected for PNDIT-F8, but for PNDIT-F3N and PNDIT-F3N-Br, weak ESR signals from the unpaired electron with a g value of 2.002 were observed (Figure 4), revealing that self-doping may occur in both of the WSCPs. Blended samples of $PC_{71}BM$/PNDIT-F8 and $PC_{71}BM$/PNDIT-F3N with the same 1:1 weight ratio were also tested to study the charge transfer properties between the two components. The samples were prepared by dissolving the same quantity of $PC_{71}BM$ and polymers in chloroform followed by drying under vacuum at 40 °C. As shown in Figure 4, no diagnostic anionic fullerene absorption could be observed in the blend of $PC_{71}BM$/PNDIT-F8, suggesting no electron transfer from PNDIT-F8 to $PC_{71}BM$. However, in the $PC_{71}BM$/PNDIT-F3N blend, strong resonance peaks with g values of 2.000 were detected. This result clearly suggests that efficient electron transfer occurred from the amine groups on the side chain of the PNDIT-F3N to $PC_{71}BM$. Because of the poor compatibility between the two materials in the $PC_{71}BM$/PNDIT-F3N-Br blend, we could not identify a suitable solvent system to prepare a thoroughly mixed blend, and therefore no accurate ESR study could be performed. However, Jen et al. have proved that bromide anions can n-dope $PC_{71}BM$ even under a mild condition, suggesting that the PNDIT-F3N-Br in our case may also n-dope the $PC_{71}BM$.[34] The results from both the SCLC and ESR

DOI: 10.1021/jacs.5b12664
J. Am. Chem. Soc. 2016, 138, 2004−2013

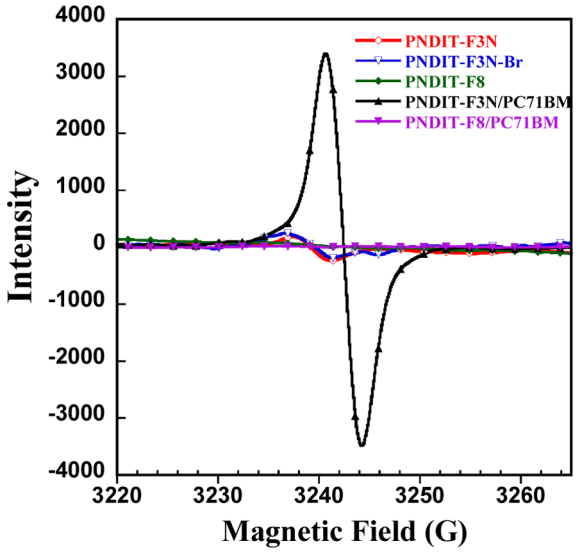

Figure 4. ESR spectra of different polymers and blends in solid state.

studies provide evidence that the amine groups and the bromide anions of the ETLs could n-dope $PC_{71}BM$ at the BHJ/ETL interface, leading to enhanced PSC device performance.

Photoconductivity Measurement. It is quite unusual for PSCs with such a thick ETL (100 nm) to operate properly unless the ETL possesses high conductivity through doping.[35] One possible doping mechanism is through photoinduced electron transfer between an electron donor and an electron acceptor, which was recently exploited in the preparation of ETLs for highly efficient PSCs.[36] To study the underlying electron transport mechanism of our ETLs, we conducted electrical measurements under both dark and illuminated conditions based on an ITO/ETL/Ag device structure (Figure 5a) to evaluate whether photoinduced doping was present in

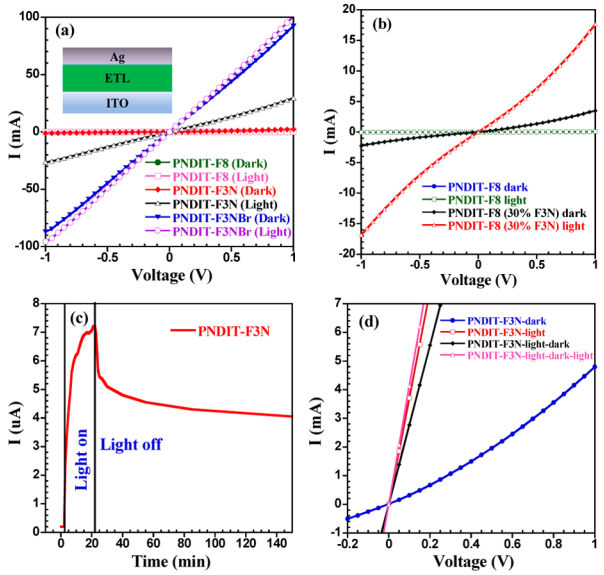

Figure 5. (a) Dark and illuminated $J-V$ characteristics of schottky-junction devices based on different ETL layers. (b) $J-V$ curves of devices for the blend film PNDIT-F8/F3N in dark and under illumination. (c) Photo current respond of the PNDIT-F3N film. (d) Dark and illuminated $J-V$ curves of the devices for the PNDIT-F3N film after the irradiation.

our systems. There was no difference in the $I-V$ characteristic of the reference polymer PNDIT-F8 when the device was measured under darkness or illumination at AM 1.5G 100 mW/cm^2, indicating that no photoinduced doping had occurred. However, for the PNDIT-F3N based devices, a distinct change in $I-V$ characteristic was observed. When the device was illuminated, the current increased significantly by about 25-fold when compared to the current in darkness at a bias of 1 V (Figure 5a). The high photoconductivity of PNDIT-F3N can be explained by the photoinduced intramolecular electron transfer from amino groups to the conjugated backbone of the polymer.[37] The proposed mechanism is described as follows: when the PNDIT-F3N is illuminated, one electron is photoexcited from the HOMO to the LUMO of the polymer, thus leaving a hole in the HOMO. As the amine contains an electron lone pair and the oxidation potential of amine (~ -5.1 eV) is smaller than the HOMO of PNDIT-F3N (-5.5 eV), electron transfer from the amine to the polymer HOMO is energetically favorable, and therefore the hole on the polymer is backfilled by the electron transferred from the amine group. As a result, a free electron remains in the LUMO of the polymer and is stable by the positively charged ammonium as a result of the photoinduced n-doping process. The stabilized n-doping effect was revealed in the $I-V$ response of the device after the removal of light as shown in Figure 5c. It was observed that when the light was on, the current increased significantly and then slowly saturated at ~7.2 μA after about 20 min of light soaking. When the light was turned off, a rapid drop in current was observed before it slowly stabilized with increasing time. After 2 h in darkness, the current (4.6 μA) maintained over 60% of the original magnitude before the light was turned off, suggesting that the n-doping effect was stabilized within the polymer. When the light was applied again to the sample, the current could be recovered as shown in Figure 5d, indicating that the photoinduced n-doping is a reversible process. To prove that the n-doping originated from the photoinduced electron transfer from the amine, we mixed the reference polymer PNDIT-F8 with the 2,7-dibromo-9,9-bis(3′-(*N*,*N*-dimethylamino)propyl)-fluorene (F3N) molecule, which is the fluorine unit with the amine-functionalized side chains building block for PNDIT-F3N, and studied the current response of the PNDIT-F8/F3N (molar ratio = 1:1) blend film. As can be seen in Figure 5b, upon light soaking, the conductivity of the blend film greatly increased, and it resembled that of the PNDIT-F3N. This finding further validated the proposed photoinduced doping mechanism for the PNDIT-F3N polymer. For the PNDIT-F3N-Br, the corresponding devices exhibited high conductivity under both the dark and illuminated conditions, indicating that the doping mechanism is different from that in the PNDIT-F3N and it is very likely, that self-doping had occurred within the material. We hypothesized that the electron from the bromine anion could transfer to the polymer and n-doped the conjugated backbone. Indeed, a similar effect was previously observed in other n-type organic semiconductors, including fullerene[20c,34] and perylene diimide molecules[38] for generating highly conductive organic films.

Transient Photocurrent. Finally, transient photocurrent measurements were used to study the competition between carrier sweep-out by the internal field and recombination during the operation of the BHJ solar cells.[39] As illustrated in Figure 6, the transient photocurrent of the PSCs with different ETLs of various thicknesses was measured at 0 bias. Devices

DOI: 10.1021/jacs.5b12664
J. Am. Chem. Soc. 2016, 138, 2004−2013

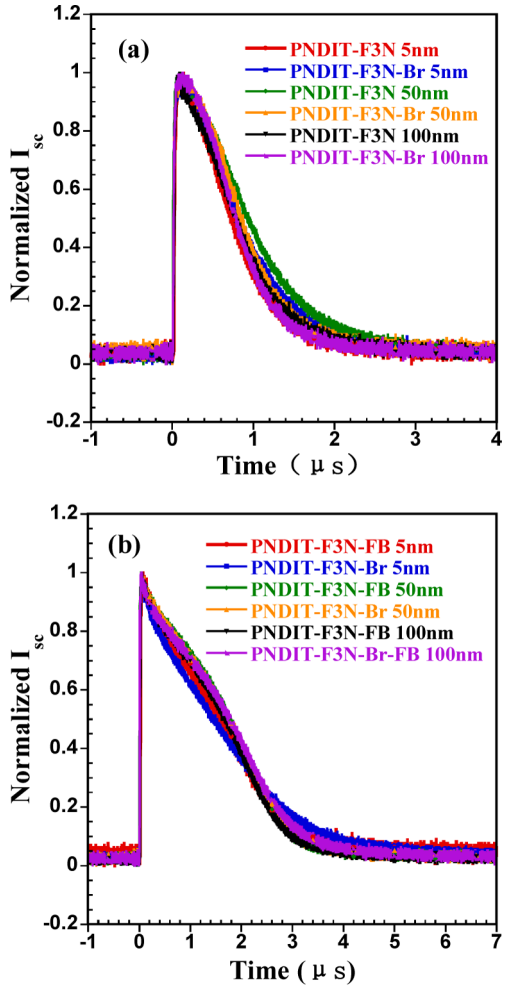

Figure 6. Transient photocurrent of different BHJ systems PTB7-Th:$PC_{71}BM$ (a) and PffBT4T-2OD/$PC_{71}BM$ (b) based PSC devices with different ETLs.

based on the PTB7-Th/$PC_{71}BM$ BHJ blend with different ETLs showed very similar decay curves, indicating that the charge extraction time is similar among all of the devices regardless of the difference in thickness of the ETLs, and this result is consistent with the high FF observed in all of the devices. The current decay times of the PffBT4T-2OD/$PC_{71}BM$-based devices were also quite similar among the devices with different ETLs and thicknesses, but in general, they were longer than those found in the PTB7-Th/$PC_{71}BM$-based devices. The longer carrier lifetime found in the PffBT4T-2OD/$PC_{71}BM$ system is understandable as higher charge mobilities were observed in the PffBT4T-2OD/$PC_{71}BM$ system,[2a] which allowed the use of a thicker active layer to produce PSCs with very high efficiency. Nevertheless, these results suggest that the thickness of the ETLs had a negligible influence on the charge extraction rate of the devices.

CONCLUSIONS

In summary, two novel n-type NDIs based WSCPs were explored for high performance PSCs. Both WSCPs possess good solubility in polar solvent, providing a facile way to process ETLs of a range of thickness with orthogonal solvents for multilayer fabrication. The π-delocalized planar structure with high electron affinity of the NDI unit enables the WSCPs to have high electron mobility and appropriate energy level alignment, which is desirable for ETLs. Both the amino and bromide-quaternized ammonium groups allow these WSCPs to possess WF tuning effects at the interface with the metal electrode and n-doping effects at the interface with the acceptor of the active layer. Interestingly, the amine-functional n-type conjugated polymer PNDIT-F3N exhibits a photoinduced conductivity-enhancing property, whereas the bromide-quaternized polymer PNDIT-F3N-Br can be self-doped with no need of light excitation. Additional studies suggested that photoinduced electron transfer from the amino groups to the NDI-based main chain plays a key role in the dramatic photo conductivity behavior of PNDIT-F3N. These results may bring new insights into the design of novel thickness-insensitive ETLs. Eventually, a high PCE of 10.11% in the PffBT4T-2OD/$PC_{71}BM$ system with conventional device structure and a prominent PCE of 8.04% with an ETL thickness of 100 nm are achieved. The specific properties of these kinds of WSCPs make them promising candidates as ETLs for use in high-performance large-area PSC modules in the future.

ASSOCIATED CONTENT

Supporting Information

The Supporting Information is available free of charge on the ACS Publications website at DOI: 10.1021/jacs.5b12664.

Complete experimental section including synthetic procedures, device fabrication and characterization details, additional UV−vis absorption spectra, cyclic voltammetry, thermal properties and atomic force micrographs. (PDF)

AUTHOR INFORMATION

Corresponding Authors

*msangusyip@scut.edu.cn
*msfhuang@scut.edu.cn

Author Contributions

†Z.W., C.S., and S.D. contributed equally.

Notes

The authors declare no competing financial interest.

ACKNOWLEDGMENTS

The work was financially supported by the Ministry of Science and Technology (No. 2014CB643500), the Natural Science Foundation of China (No. 51521002, 21520102006, 21490573, 51323003, and 21125419), Guangdong Innovative Research Team Program of China (No. 201101C0105067115) and Guangdong Natural Science Foundation (Grant No. S2012030006232).

REFERENCES

(1) (a) Thompson, B. C.; Fréchet, J. M. J. *Angew. Chem., Int. Ed.* **2008**, *47*, 58. (b) Beaujuge, P. M.; Fréchet, J. M. J. *J. Am. Chem. Soc.* **2011**, *133*, 20009. (c) Li, Y. *Acc. Chem. Res.* **2012**, *45*, 723. (d) Li, G.; Zhu, R.; Yang, Y. *Nat. Photonics* **2012**, *6*, 153. (e) Dou, L.; You, J.; Hong, Z.; Xu, Z.; Li, G.; Street, R. A.; Yang, Y. *Adv. Mater.* **2013**, *25*, 6642. (f) Huang, Y.; Kramer, E. J.; Heeger, A. J.; Bazan, G. C. *Chem. Rev.* **2014**, *114*, 7006. (g) Heeger, A. J. *Adv. Mater.* **2014**, *26*, 10.

(2) (a) Liu, Y.; Zhao, J.; Li, Z.; Mu, C.; Ma, W.; Hu, H.; Jiang, K.; Lin, H.; Ade, H.; Yan, H. *Nat. Commun.* **2014**, *5*, 5293. (b) Liao, S.-H.; Jhuo, H.-J.; Yeh, P.-N.; Cheng, Y.-S.; Li, Y.-L.; Lee, Y.-H.; Sharma, S.; Chen, S.-A. *Sci. Rep.* **2014**, *4*, 6813. (c) Chen, C. C.; Chang, W. H.; Yoshimura, K.; Ohya, K.; You, J. B.; Gao, J.; Hong, Z. R.; Yang, Y. *Adv. Mater.* **2014**, *26*, 5670. (d) Yusoff, A. R. b. M.; Kim, D.; Kim, H. P.; Shneider, F. K.; da Silva, W. J.; Jang, J. *Energy Environ. Sci.* **2015**, *8*,

DOI: 10.1021/jacs.5b12664
J. Am. Chem. Soc. 2016, 138, 2004−2013

303. (e) Vohra, V.; Kawashima, K.; Kakara, T.; Koganezawa, T.; Osaka, I.; Takimiya, K.; Murata, H. *Nat. Photonics* **2015**, *9*, 403. (f) Jagadamma, L. K.; Al-Senani, M.; El-Labban, A.; Gereige, I.; Ngongang Ndjawa, G. O.; Faria, J. C. D.; Kim, T.; Zhao, K.; Cruciani, F.; Anjum, D. H.; McLachlan, M. A.; Beaujuge, P. M.; Amassian, A. *Adv. Energy Mater.* **2015**, *5*, 1500204. (g) He, Z.; Xiao, B.; Liu, F.; Wu, H.; Yang, Y.; Xiao, S.; Wang, C.; Russell, T. P.; Cao, Y. *Nat. Photonics* **2015**, *9*, 174. (h) Chen, J. D.; Cui, C.; Li, Y. Q.; Zhou, L.; Ou, Q. D.; Li, C.; Li, Y.; Tang, J. X. *Adv. Mater.* **2015**, *27*, 1035.

(3) (a) Stuart, A. C.; Tumbleston, J. R.; Zhou, H.; Li, W.; Liu, S.; Ade, H.; You, W. *J. Am. Chem. Soc.* **2013**, *135*, 1806. (b) Helgesen, M.; Carlé, J. E.; Krebs, F. C. *Adv. Energy Mater.* **2013**, *3*, 1664. (c) Hu, X.; Yi, C.; Wang, M.; Hsu, C.-H.; Liu, S.; Zhang, K.; Zhong, C.; Huang, F.; Gong, X.; Cao, Y. *Adv. Energy Mater.* **2014**, *4*, 1400378. (d) Armin, A.; Hambsch, M.; Wolfer, P.; Jin, H.; Li, J.; Shi, Z.; Burn, P. L.; Meredith, P. *Adv. Energy Mater.* **2015**, *5*, 1401221. (e) Adams, J.; Spyropoulos, G. D.; Salvador, M.; Li, N.; Strohm, S.; Lucera, L.; Langner, S.; Machui, F.; Zhang, H.; Ameri, T.; Voigt, M. M.; Krebs, F. C.; Brabec, C. J. *Energy Environ. Sci.* **2015**, *8*, 169. (f) Duan, C.; Huang, F.; Cao, Y. *Polym. Chem.* **2015**, *6*, 8081.

(4) (a) Hoven, C. V.; Garcia, A.; Bazan, G. C.; Nguyen, T.-Q. *Adv. Mater.* **2008**, *20*, 3793. (b) Jiang, H.; Taranekar, P.; Reynolds, J. R.; Schanze, K. S. *Angew. Chem., Int. Ed.* **2009**, *48*, 4300. (c) Huang, F.; Wu, H.; Cao, Y. *Chem. Soc. Rev.* **2010**, *39*, 2500. (d) Duan, C.; Zhang, K.; Zhong, C.; Huang, F.; Cao, Y. *Chem. Soc. Rev.* **2013**, *42*, 9071. (e) Chueh, C.-C.; Li, C.-Z.; Jen, A. K.-Y. *Energy Environ. Sci.* **2015**, *8*, 1160.

(5) Zhang, K.; Zhong, C.; Liu, S.; Mu, C.; Li, Z.; Yan, H.; Huang, F.; Cao, Y. *ACS Appl. Mater. Interfaces* **2014**, *6*, 10429.

(6) Heywang, G.; Jonas, F. *Adv. Mater.* **1992**, *4* (2), 116.

(7) (a) Zhou, H.; Zhang, Y.; Mai, C. K.; Collins, S. D.; Nguyen, T. Q.; Bazan, G. C.; Heeger, A. J. *Adv. Mater.* **2014**, *26*, 780. (b) Zhou, H.; Zhang, Y.; Mai, C. K.; Collins, S. D.; Bazan, G. C.; Nguyen, T. Q.; Heeger, A. J. *Adv. Mater.* **2015**, *27*, 1767.

(8) (a) Luo, J.; Wu, H.; He, C.; Li, A.; Yang, W.; Cao, Y. *Appl. Phys. Lett.* **2009**, *95*, 043301. (b) Zhao, Y.; Xie, Z. Y.; Qin, C. J.; Qu, Y.; Geng, Y. H.; Wang, L. X. *Sol. Energy Mater. Sol. Cells* **2009**, *93*, 604. (c) Na, S. I.; Oh, S. H.; Kim, S. S.; Kim, D. Y. *Org. Electron.* **2009**, *10*, 496.

(9) Huang, F.; Wu, H.; Wang, D.; Yang, W.; Cao, Y. *Chem. Mater.* **2004**, *16*, 708.

(10) Zheng, H.; Zheng, Y.; Liu, N.; Ai, N.; Wang, Q.; Wu, S.; Zhou, J.; Hu, D.; Yu, S.; Han, S.; Xu, W.; Luo, C.; Meng, Y.; Jiang, Z.; Chen, Y.; Li, D.; Huang, F.; Wang, J.; Peng, J.; Cao, Y. *Nat. Commun.* **2013**, *4*, 1971.

(11) (a) Zuo, L.; Chang, C.-Y.; Chueh, C.-C.; Zhang, S.; Li, H.; Jen, A. K. Y.; Chen, H. *Energy Environ. Sci.* **2015**, *8*, 1712. (b) Zheng, Z.; Zhang, S.; Zhang, M.; Zhao, K.; Ye, L.; Chen, Y.; Yang, B.; Hou, J. *Adv. Mater.* **2015**, *27*, 1189.

(12) (a) You, J.; Yang, Y.; Hong, Z.; Song, T.-B.; Meng, L.; Liu, Y.; Jiang, C.; Zhou, H.; Chang, W.-H.; Li, G.; Yang, Y. *Appl. Phys. Lett.* **2014**, *105*, 183902. (b) Xue, Q.; Hu, Z.; Liu, J.; Lin, J.; Sun, C.; Chen, Z.; Duan, C.; Wang, J.; Liao, C.; Lau, W. M.; Huang, F.; Yip, H.-L.; Cao, Y. *J. Mater. Chem. A* **2014**, *2*, 19598.

(13) (a) Liu, Y.; Page, Z. A.; Russell, T. P.; Emrick, T. *Angew. Chem., Int. Ed.* **2015**, *54*, 11485. (b) Hu, L.; Wu, F.; Li, C.; Hu, A.; Hu, X.; Zhang, Y.; Chen, L.; Chen, Y. *Macromolecules* **2015**, *48*, 5578.

(14) Sun, C.; Wu, Z. H.; Yip, H.-L.; Zhang, H.; Jiang, X.-F.; Xue, Q. F.; Hu, Z. C.; Hu, Z. H.; Shen, Y.; Wang, M. K.; Huang, F.; Cao, Y. *Adv. Energy Mater.* **2015**, 1501534.

(15) Yan, H.; Chen, Z.; Zheng, Y.; Newman, C.; Quinn, J. R.; Dotz, F.; Kastler, M.; Facchetti, A. *Nature* **2009**, *457*, 679.

(16) Bucella, S. G.; Luzio, A.; Gann, E.; Thomsen, L.; McNeill, C. R.; Pace, G.; Perinot, A.; Chen, Z. H.; Facchetti, A.; Caironi, M. *Nat. Commun.* **2015**, *6*, 8394.

(17) (a) Facchetti, A. *Mater. Today* **2013**, *16*, 123. (b) Mu, C.; Liu, P.; Ma, W.; Jiang, K.; Zhao, J. B.; Zhang, K.; Chen, Z. H.; Wei, Z. H.; Yi, Y.; Wang, J. S.; Yang, S. H.; Huang, F.; Facchetti, A.; Ade, H.; Yan, H. *Adv. Mater.* **2014**, *26*, 7224. (c) Fabiano, S.; Himmelberger, S.; Drees, M.; Chen, Z.; Altamimi, R. M.; Salleo, A.; Loi, M. A.; Facchetti, A. *Adv. Energy Mater.* **2014**, *4*, 1301409.

(18) Steyrleuthner, R.; Di Pietro, R.; Collins, B. A.; Polzer, F.; Himmelberger, S.; Schubert, M.; Chen, Z.; Zhang, S.; Salleo, A.; Ade, H.; Facchetti, A.; Neher, D. *J. Am. Chem. Soc.* **2014**, *136*, 4245.

(19) Liang, Y. L.; Chen, Z. H.; Jing, Y.; Rong, Y. G.; Facchetti, A.; Yao, Y. *J. Am. Chem. Soc.* **2015**, *137*, 4956.

(20) (a) Yip, H.-L.; Jen, A. K. Y. *Energy Environ. Sci.* **2012**, *5*, 5994. (b) Yang, T.; Wang, M.; Duan, C.; Hu, X.; Huang, L.; Peng, J.; Huang, F.; Gong, X. *Energy Environ. Sci.* **2012**, *5*, 8208. (c) Li, C. Z.; Chang, C. Y.; Zang, Y.; Ju, H. X.; Chueh, C. C.; Liang, P. W.; Cho, N.; Ginger, D. S.; Jen, A. K. *Adv. Mater.* **2014**, *26*, 6262.

(21) Ahmed, E.; Ren, G.; Kim, F. S.; Hollenbeck, E. C.; Jenekhe, S. A. *Chem. Mater.* **2011**, *23*, 4563.

(22) (a) Balanda, P. B.; Ramey, M. B.; Reynolds, J. R. *Macromolecules* **1999**, *32*, 3970. (b) Huang, F.; Hou, L.; Wu, H.; Wang, X.; Shen, H.; Cao, W.; Yang, W.; Cao, Y. *J. Am. Chem. Soc.* **2004**, *126*, 9845.

(23) Liu, B.; Yu, W. L.; Lai, Y. H.; Huang, W. *Macromolecules* **2002**, *35*, 4975.

(24) (a) Woo, H. Y.; Liu, B.; Kohler, B.; Korystov, D.; Mikhailovsky, A.; Bazan, G. C. *J. Am. Chem. Soc.* **2005**, *127*, 14721. (b) Cheng, Y.-J.; Yang, S.-H.; Hsu, C.-S. *Chem. Rev.* **2009**, *109*, 5868.

(25) Henson, Z. B.; Zhang, Y.; Nguyen, T. Q.; Seo, J. H.; Bazan, G. C. *J. Am. Chem. Soc.* **2013**, *135*, 4163.

(26) (a) Pavlishchuk, V. V.; Addison, A. W. *Inorg. Chim. Acta* **2000**, *298*, 97. (b) Hwang, Y.-J.; Earmme, T.; Courtright, B. A. E.; Eberle, F. N.; Jenekhe, S. A. *J. Am. Chem. Soc.* **2015**, *137*, 4424.

(27) Li, Y.; Cao, Y.; Gao, J.; Wang, D.; Yu, G.; Heeger, A. J. *Synth. Met.* **1999**, *99*, 243.

(28) (a) Schottel, B. L.; Chifotides, H. T.; Dunbar, K. R. *Chem. Soc. Rev.* **2008**, *37*, 68. (b) Song, Q.; Li, F.; Wang, Z.; Zhang, X. *Chem. Sci.* **2015**, *6*, 3342.

(29) (a) Li, C. Z.; Chueh, C. C.; Yip, H.-L.; Ding, F. Z.; Li, X. S.; Jen, A. K. Y. *Adv. Mater.* **2013**, *25*, 2457. (b) Duan, C.; Cai, W.; Hsu, B. B.; Zhong, C.; Zhang, K.; Liu, C.; Hu, Z.; Huang, F.; Bazan, G. C.; Heeger, A. J. *Energy Environ. Sci.* **2013**, *6*, 3022. (c) Cho, N.; Yip, H.-L.; Davies, J. A.; Kazarinoff, P. D.; Zeigler, D. F.; Durban, M. M.; Segawa, Y.; O'Malley, K. M.; Luscombe, C. K.; Jen, A. K.-Y. *Adv. Energy Mater.* **2011**, *1*, 1148. (d) Zhang, Z.-G.; Qi, B.; Jin, Z.; Chi, D.; Qi, Z.; Li, Y.; Wang, J. *Energy Environ. Sci.* **2014**, *7*, 1966.

(30) Liao, S.-H.; Li, Y.-L.; Jen, T.-H.; Cheng, Y.-S.; Chen, S.-A. *J. Am. Chem. Soc.* **2012**, *134*, 14271.

(31) (a) Zhou, H.; Zhang, Y.; Seifter, J.; Collins, S. D.; Luo, C.; Bazan, G. C.; Nguyen, T. Q.; Heeger, A. J. *Adv. Mater.* **2013**, *25*, 1646. (b) Zhang, K.; Hu, Z.; Duan, C.; Ying, L.; Huang, F.; Cao, Y. *Nanotechnology* **2013**, *24*, 484003.

(32) Zhang, K.; Hu, Z.; Xu, R.; Jiang, X.-F.; Yip, H.-L.; Huang, F.; Cao, Y. *Adv. Mater.* **2015**, *27*, 3607.

(33) Mihailetchi, V.; Wildeman, J.; Blom, P. *Phys. Rev. Lett.* **2005**, *94*, 126602.

(34) Li, C. Z.; Chueh, C. C.; Ding, F.; Yip, H.-L.; Liang, P. W.; Li, X.; Jen, A. K. Y. *Adv. Mater.* **2013**, *25*, 4425.

(35) Walzer, K.; Maennig, B.; Pfeiffer, M.; Leo, K. *Chem. Rev.* **2007**, *107*, 1233.

(36) Nian, L.; Zhang, W.; Zhu, N.; Liu, L.; Xie, Z.; Wu, H.; Würthner, F.; Ma, Y. *J. Am. Chem. Soc.* **2015**, *137*, 6995.

(37) Che, Y.; Yang, X.; Liu, G.; Yu, C.; Ji, H.; Zuo, J.; Zhao, J.; Zang, L. *J. Am. Chem. Soc.* **2010**, *132*, 5743.

(38) Russ, B.; Robb, M. J.; Brunetti, F. G.; Miller, P. L.; Perry, E. E.; Patel, S. N.; Ho, V.; Chang, W. B.; Urban, J. J.; Chabinyc, M. L.; Hawker, C. J.; Segalman, R. A. *Adv. Mater.* **2014**, *26*, 3473.

(39) Cowan, S. R.; Street, R.; Cho, S.; Heeger, A. *Phys. Rev. B: Condens. Matter Mater. Phys.* **2011**, *83*, 035205.

DOI: 10.1021/jacs.5b12664
J. Am. Chem. Soc. 2016, 138, 2004−2013